Simplified Model for Heat Transport for Cables in Pipes

Svein M. Hellesø and Espen Eberg

***Abstract*—This paper addresses challenges with modeling of heat transfer phenomenon for cables in duct or pipes when applying a numerical solution. Heat transport mechanisms between the cable and pipe surfaces are conduction, convection and radiation. Numerical calculation of convection when applying a finite element analysis (FEA), or other numerical tools requires heavy computation power and great skills of the program operator. In general, this is the most difficult part when modeling the heat transfer between the cable and the pipe surfaces and practitioners are often forced to use simplifications or approximate models. This paper introduces a simplified model where the contribution from convection is replaced by a heat source at the pipe wall and a corresponding heat sink at the cable. The phenomenon of air rising vertically in the tube resulting in the upper half of the pipe being heated more by convection than the lower half is also modelled. The simplified model is compared to both known models from thermodynamics, FEA including convection and laboratory as well as the full-scale field measurements. The simplified model shows good correspondence to both simulations and measurements, with the temperatures deviating by less than 1 °C.**

***Index Terms*—Power cables, ampacity calculations, cables in pipes and ducts, modeling.**

I. Introduction

In MANY cities around the world, medium- and low-voltage cables are often located in duct banks to allow a large number of circuits to be laid in the same trench or are installed in ducts for protection and easy replacement. Ampacity calculations of such cables involve analysis of the heat transfer phenomena between the cable surface and the duct or pipe wall. This heat transfer takes three forms: conduction, convection, and radiation. It is a well-documented fact that the radiation plays the predominant role in this process, while the convection is the most difficult to model, [1]. The empirical formula for the thermal resistance of the air inside the duct given in the IEC Standard 60287-2-1, [2], does not take into account the amount of air inside the pipe and was developed for ducts up to 50 cm in diameter. Another important assumption is that the cables are located in the center of the duct, which in reality is almost never the case since they are usually placed at its bottom.

Manuscript received 2 September 2021; revised 24 November 2021; accepted 18 December 2021. Date of publication 23 December 2021; date of current version 23 September 2022. This work was supported by the partners of the DynKap R&D-Project and Norwegian Research Council under Grant 296215. Paper no. TPWRD-01322-2021. *(Corresponding author: Espen Eberg.)*

The authors are with SINTEF Energy Research, 7034 Trondheim, Norway (e-mail: svein.helleso@sintef.no; espen.eberg@sintef.no).

Color versions of one or more figures in this article are available at https://doi.org/10.1109/TPWRD.2021.3137876.

Digital Object Identifier 10.1109/TPWRD.2021.3137876

Literature on modelling of cables in ducts is extensive, and only the most recent contributions are reviewed here. The most comprehensive recent analysis of the heat transfer phenomena for cables installed in ducts can be found in [3] and [4]. The authors of [3] reported an in-depth investigation, which led to the conclusion that the source of the discrepancy between the measured temperatures and the values obtained by applying the IEC standard is a result of an inaccuracy in the calculation of the heat transfer of the air between the cable and the internal duct surfaces. The authors found that standard calculations simplify the problem too much, resulting in relatively large errors. A more precise formulation, yet simple enough for a computer implementation, is proposed in this paper.

Degefa *et al.* [4], performed several FEA (Finite Element Analysis) simulations and tests to point out the weaknesses in the IEC formulation. However, as pointed out in [3], the correlations cited in [4], taken from [5], fail when the gap between the cable and duct is larger than 0.3 times the diameter of the cable.

Other recent references analyze cables in ducts but do not focus on the accuracy of the heat transfer by the convection in the pipes and ducts. Lu *et al.* [6], present a temperature field model of a cable group inside a duct applying FEA. References [7] and [8] present a heat transfer matrix and superimposed thermal field-based method for calculation of the steady state temperature rises in three-core cable groups laid in duct. de Leon examines in [9], among other parameters, the effect of the duct size on cable ampacity.

Vaucheret *et al.* [10], examined the heat transfer for extruded cables in short sections of conduit by using FEA software to determine ampacity derating as a function of the conduit length, soil resistivity, burial depth, and the number of cables in the conduit. The heat transport in the conduit was calculated according to [11]. The effect of conduit length is also studied in [12], where heat transport in the duct is calculated according to the IEC 60287-2-1 for the simplified quasi-3D model, while FEA is used as a reference for evaluation of the simplified model – both placing the cable in the center of the pipe.

This paper proposes an application of a more computationally efficient FEA approach in rating of electric power cables installed in conduits, ducts or pipes,[1] rather than suggesting corrections to the IEC 60287 as was done, for example in [3]. The FEA software, especially COMSOL Multiphysics, is a tool that is used more and more often to overcome the limitations

[1]The word pipe will be used throughout in what follows, denoting conduits, ducts and pipes).

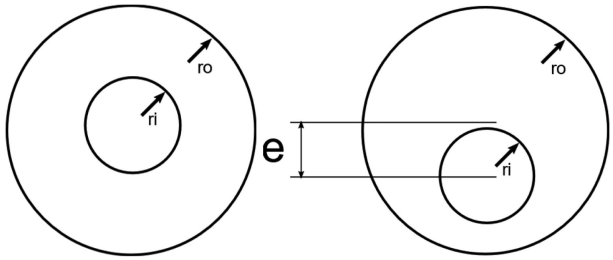

Fig. 1. Cable inside a pipe: concentric and eccentric configurations.

of the analytical methods. By implementing the models in such tools, flexibility to address complex trench geometries can be ensured. As might be attested by many practitioners, this tool can be difficult to use and requires an in-depth knowledge of the heat transfer modelling techniques. Correct description of the heat transfer by convection is by many considered the most challenging task and is also a part of the FEA that requires most computational power. By combining computationally simplified models with a pre-built graphical user interface, cable rating calculations applying FEA can be adopted by practitioners and utilities in a simple way [13].

This paper introduces a simple model, that can be used in a FEA software, that accurately represents the reality of heat transfer in the air-filled pipes. The emphasis is on the conductive and convective heat transfer, whereas [3] concentrated solely on the convective phenomenon. The existing models are described in Chapter II followed by the development of the new model implemented in FEA in Chapters III and IV. Chapter V and VI describes the model verification procedure by experimental setups in the laboratory and in a full-scale measurement of a road crossing. Both numerical examples and measurements demonstrate the accuracy of the proposed model.

II. Heat Transport Between Cable and Pipe

There are three mechanisms for heat transfer between a cable and a pipe: conduction, convection and radiation. Conduction and convection are described here since the radiative heat transfer is well understood and described in many sources, e.g., [14].

A. Conduction

The heat transfer by conduction is, in principle, given by the following differential equation:

$$q = -k\nabla T \tag{1}$$

where:

q	is the vector of the heat flux (W/m^2),
k	is the thermal conductivity (W/m.K), and
∇T	is the gradient operator on the temperature field T (K).

For some simple geometries and boundary conditions, it is possible to find analytical solutions of (1). For example, in a concentric configuration having isothermal surfaces with internal and external radii r_i and r_o , respectively (see Fig. 1), the conduction heat transfer is given by:

$$q_{cond} = 2\pi k_{air} \frac{T_i - T_o}{\ln \frac{r_o}{r_i}} = h_c \ (T_i - T_o) \tag{2}$$

where h_c is the corresponding heat transfer coefficient.

For an eccentric configuration with an offset *e* (see Fig. 1), the conduction heat transfer (assuming isothermal surfaces) is [14]:

$$q_{cond,e} = \frac{2\pi k_{air} \left(T_i - T_o\right)}{\ln \frac{r_o}{r_i}} \frac{\ln \frac{r_o}{r_i}}{\cosh^{-1}\left(\frac{D_o^2 + D_i^2 - 4e^2}{2D_o D_i}\right)} = h_{c,e} \ (T_i - T_o) \tag{3}$$

with D_i and D_o the internal and external diameters, and $h_{c,e}$ is the corresponding heat transfer coefficient.

For an offset *e* that approaches the maximum value, i.e., the inner cylinder almost touching the outer cylinder, the heat transfer increases significantly, and at when the two cylinders touch, the heat transfer tends to infinity. In practice, the finite thermal conductivity of the materials of the cable and the pipe limits the maximum heat transfer between them and the assumption of the isothermal surfaces breaks down.

B. Convection

Heat transport by convection between concentric isothermal surfaces have been thoroughly described in the literature, and correction factors for the increased efficiency of heat transport including convection have been established.

For concentric cylinders, the effective thermal conductivity of the air between the cable and inner pipe surfaces is given by [15]:

$$k_{eff} = 0.386 \cdot k_{air} \cdot \left(\frac{Pr}{0.861 + Pr}\right)^{1/4} Ra_{cyl}^{1/4} \tag{4}$$

with

$$Ra_{cyl} = \frac{\left(\ln \frac{D_o}{D_i}\right)^4}{L^3\left(D_i^{-3/5} + D_o^{-3/5}\right)^5} Ra_L \tag{5}$$

$$L = \frac{D_o - D_i}{2} \tag{6}$$

$$Ra_L = \frac{g\beta L^3 \Delta T}{\nu a} \tag{7}$$

where:

Pr	is the Prandtl number (-),
g	is acceleration due to gravity (m/s^2),
β	is volumetric thermal expansion coefficient (1/K),
ν	is kinematic viscosity of air (m^2/s), and
a	is thermal diffusivity of air (m^2/s).

All material parameters are evaluated at the mean air temperature and isothermal surfaces are assumed.

Kuehn and Goldstein, [16], have developed a method for modeling the heat transfer between two cylindrical surfaces

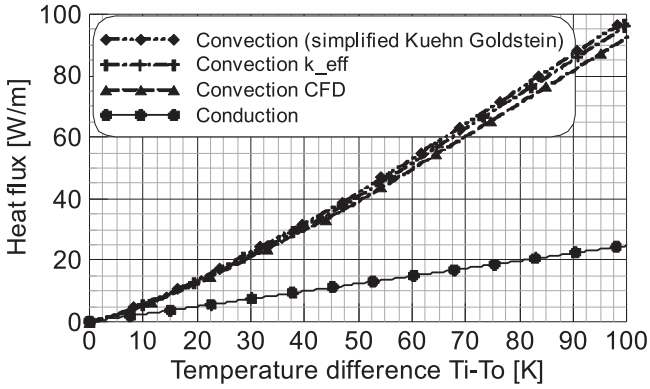

Fig. 2. Comparison of heat transport by conduction and convection based on the relationships from literature and direct computation by the FEA. Convection k_{eff} is based on (4), the simplified Kuhen & Goldstein is based on [16].

that includes a slight eccentricity. A simplified version of their method, valid for laminar convective flow, has been developed by Teertstra and Yovanovich [17].

Sandia National Laboratories has also presented a thorough review of the correction factors for convection in the annulus in horizontal concentric cylinders [18] and has shown how corrections factors for other geometries can be established [19].

The convective model discussed in this chapter is the same as used in [4]; hence, one is to be aware of its limitations as discussed in the Introduction.

III. Setup of the FEA Verification Procedure

To verify that the FEA used in the further development reproduces the heat transfer between the cables and pipes correctly, the first task was to compare the numerical studies with the result published in the literature. FEA studies that includes convection have been performed for concentric and eccentric sample geometries and compared with the published models. Fig. 2 shows the heat flux values computed with different methods as a function of the temperature difference between the two surfaces for a concentric geometry with $D_i = 55$ mm and $D_o = 110$ mm.

These results show that the values from the FEA are in good correspondence with the Kuehn and Goldstein correlations, which implies that the FEA also is in good correspondence with the real conditions. We can also observe that for the case of concentric and isothermal surfaces, convection increases heat transport by a factor of 2.6 with a temperature difference of 20 °C compared to conduction.

Fig. 3 and Fig. 4 show the calculated temperature profiles and air flow by the FEA for concentric and eccentric geometries, respectively.

For eccentric geometries, the situation is different, since the heat transport by conduction increases as the eccentricity increases, until the cable touches the pipe. The contribution from convection as a function of the temperature difference between the inner and outer cylinders is shown in Fig. 5. It can be seen that with a gap of 1 mm, isothermal surfaces and a temperature

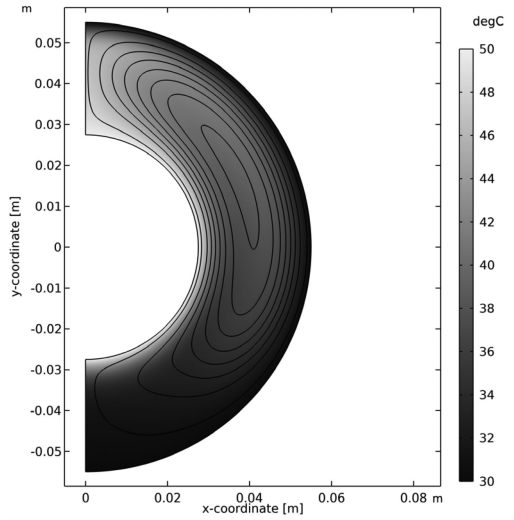

Fig. 3. Temperature and airflow/streamlines for concentric geometry from FEA with $\Delta T = 20$ °C, $D_i = 55$ mm and $D_0 = 110$ mm.

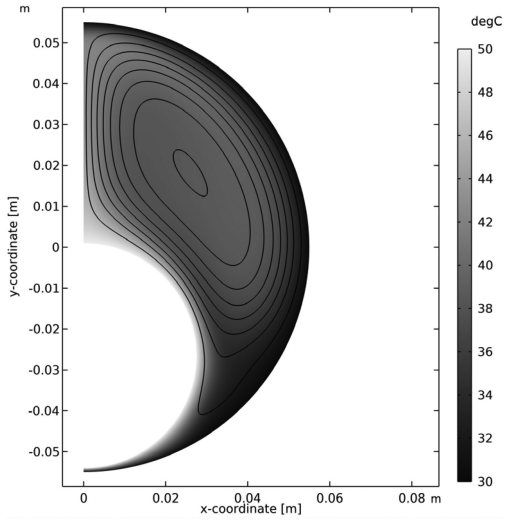

Fig. 4. Temperature and airflow for eccentric geometry from the FEA with $\Delta T = 20$ °C, $D_i = 55$ mm, $D_0 = 110$ mm and minimum gap between inner and outer cylinders of approximately 1 mm.

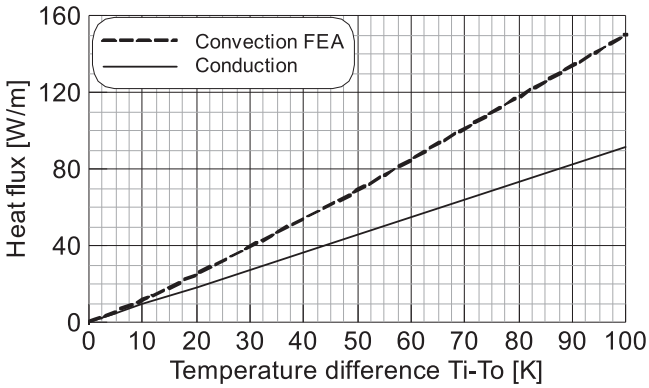

Fig. 5. Heat transfer by convection from direct fluid flow simulation with FEA, and heat transfer by conduction only, for the geometry in Fig. 4.

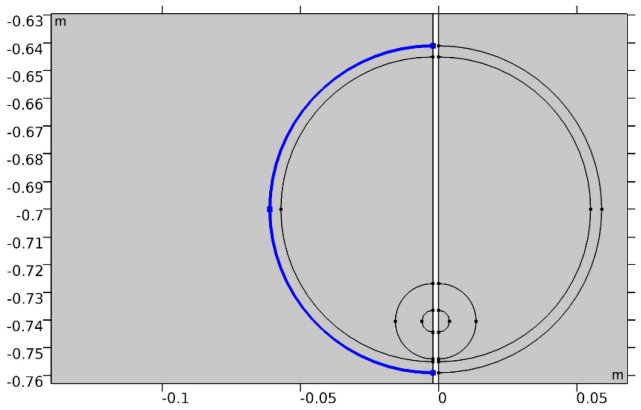

Fig. 6. Location of the heat source on the pipe wall.

difference of 20 °C, the convection contribution gives an increase in a heat transport by a factor of 1.37 comparing to conduction.

IV. Simplified FEA Model Including Convection Contribution

A. Single Cable Formation

A simplified FEA model that includes contribution from convection in the eccentric geometries has been developed. As a basis for the calculations, a standard cable trench with 0.7 m burial depth has been used with the soil thermal resistivity of 1.0 m.K/W and the temperature of 15 °C at the ground surface.

The procedure uses the calculations described above in (6-9) as a starting point. From this, the following procedure is applied:

1) Average temperatures for the cable outer and the pipe inner surfaces are found (T_o and T_i) .
2) The material properties of air are found for the average temperature ($T_m = (T_i + T_o)\ /2$) .
3) An effective thermal conductivity is found from (4).
4) The heat contribution from convection is found. For typical cable/pipe geometries, the best fit was found by using a correction factor of 0.4 on the contribution from convection for the concentric configuration with isothermal surfaces. Thus,

$$Q_{conv} = \ 0.4k_{air}\left(\frac{k_{eff}}{kk_{air}} - 1\right)\Delta T \ln\frac{D_o}{D_i} \qquad (8)$$

5) The heat contribution is added as a distributed heat source to the pipe surface and subtracted as a distributed heat sink on the conductor. The location of the heat source is shown in Fig. 6 and the flux density is given by:

$$q_{pipe} = \frac{Q_{conv}}{\pi D_o} \qquad (9)$$

The expressions for k_{eff} and the Rayleigh-numbers are as before, and average temperatures are used for the surface and pipe wall (4) – (7).

For isothermal concentric surfaces, the temperature field in the gap is not determined when using (6) to account for the effect of convection on the heat flow. The heat flow can thus be viewed as being removed from the inner surface and added to the outer surface. For isothermal surfaces, the distribution of the heat source and sink is of little consequence as the assumption of isothermal surfaces implies infinite thermal conductivity tangentially to the inner and outer surfaces, which for metallic pipes might be a good approximation. For non-metallic pipes, e.g., polymer pipes with significantly lower thermal conductivity, the distribution of the heat source along the surface has more influence on the actual temperature field, as the assumption of isothermal surfaces is much less appropriate. For the heat sink at the conductor there is less need for careful consideration of the actual location of the heat sink, due to the high thermal conductivity resulting in uniform temperature over the cross section on conductors.

TABLE I
Calculated Temperature of the Conductor and Pipe Wall With Defined Heat Source in the Conductor

	r_i/r_o	Q_{cond} [W/m]	T_{cond} [°C]	T_{bottom} [°C]	T_{side} [°C]	T_{top} [°C]
Full FEA	0.1	28.0	90.0	36.0	28.1	28.6
	0.5	50.2	90.0	46.4	39.6	40.3
	0.9	58.9	90.0	48.4	44.4	42.9
Simplified model	0.1	28.0	1.0 %	6.4 %	0.0 %	-5.6 %
	0.5	50.2	0.9 %	3.0 %	-0.5 %	-7.7 %
	0.9	58.9	0.1 %	0.2 %	0.0 %	-1.2 %
Ref. [3]	0.1	28.0	1.0 %	6.4 %	0.0 %	-5.6 %
	0.5	50.2	0.9 %	3.0 %	-0.5 %	-7.7 %
	0.9	58.9	0.1 %	0.2 %	0.0 %	-1.2 %

For the simplified model and results based on Ref. [3], the temperatures are given relative to full FEA in percentages.

Numerous simulations were performed and, for a large range of ratios between the cable and pipe diameters, this method gives a deviation of the conductor temperature smaller than 1 °C compared to the FEA that includes full calculation of convection. The deviations at r_i/r_o ratios 0.1, 0.5 and 0.9 between the proposed simplified model, the simplified model in [3], and the full FEA model are given in Table I for a heat source in the conductor that gave the conductor temperature of 90 °C in the full FEA model. The deviation in temperature on the conductor is relatively small (1 °C / 1%), and for a single cable installation, the proposed model will provide feasible results that are more accurate compared to both the IEC and the proposed enhancement in [3]. For the temperatures around the pipe, the deviation is larger at the top and bottom of the pipe wall compared to full FEA, where the maximum deviation exceeds 3.0 °C, as illustrated in Fig. 7. It should be noted that on the side of the pipe, which according to [3] corresponds to the location where the average temperature is found, the deviation from the full FEA model is negligible.

To improve the accuracy of the temperature distribution on the pipe wall, a heat source following the angular hyperbolic tangent function, $\tan h(\varphi)$, is introduced, as heat distribution along the pipe wall from full FEA simulations is close to this distribution. $\tan h(\varphi)$ is asymmetric with respect to φ , hence a constant factor was added to the expression in order to provide net heat transfer from the conductor to pipe wall:

$$q_{distr} = \ 4 \cdot q_{pipe} \tanh(\varphi) + q_{pipe} \qquad (10)$$

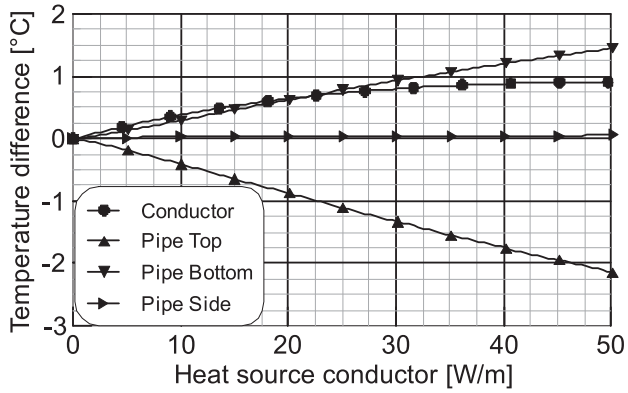

Fig. 7. Difference in the temperature between the FEA using full convection calculation and the simplified model without the tanh(φ) variation of the heat source along the pipe wall.

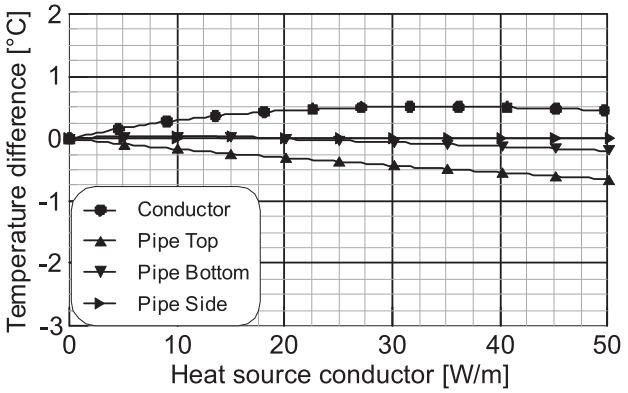

Fig. 10. Difference in the temperature between the FEA using full convection calculation and simplified model with *tanh(φ)* variation of the heat source along the pipe wall.

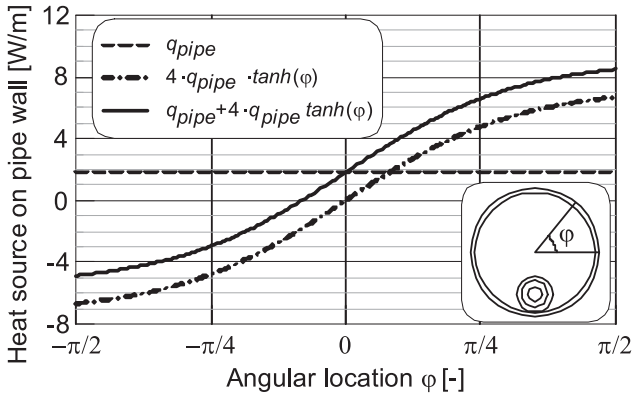

Fig. 8. Distribution of a heat source on the pipe wall to represent convective heat transfer. The broken line is given by eq (9), the dotted-broken line is the tanh-variation and the solid line is the summation of these two terms as provided in (10).

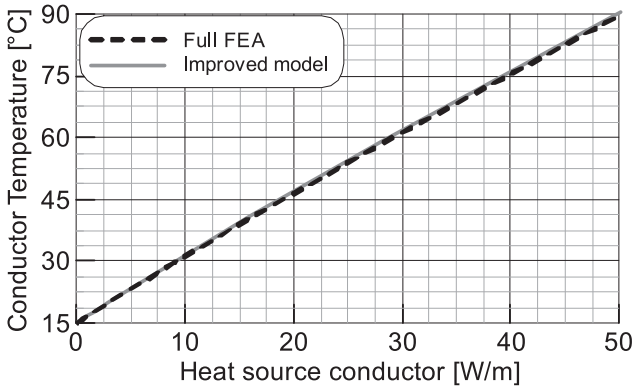

Fig. 9. Conductor temperature from calculating convection with the full COMSOL model and from the improved model. Pipe diameter is 110 mm and cable diameter is 55 mm.

where q_{pipe} is defined by (9). The resulting distribution of the heat on the pipe wall is shown in Fig. 8. Intregrating (10) for $\varphi \in \langle 0, 2\pi \rangle$ will give the same net heat as in (9).

Fig. 9 shows the conductor temperature as function of conductor loss for the improved model and full FEA calculation for r_i/r_o = 27.5 mm / 55 mm = 0.5. Fig. 10 displays the deviations for

TABLE II
COMPARISON OF THE IMPROVED SIMPLIFIED MODEL AND FULL FEA CALCULATION

	r_i/r_o	Q_{cond} [W/m]	T_{cond} [°C]	T_{bottom} [°C]	T_{side} [°C]	T_{top} [°C]
Full FEA	0.1	28.0	90.0	36.0	28.1	28.6
	0.5	50.2	90.0	46.4	39.6	40.3
	0.9	58.9	90.0	48.4	44.4	42.9
Simplified model	0.1	28.0	0.2 %	0.8 %	-0.4 %	0.7 %
	0.5	50.2	0.4 %	-0.6 %	-0.5 %	-4.0 %
	0.9	58.9	0.1 %	0.2 %	0.0 %	-1.2 %

For the simplified model the temperatures are given relative to full FEA in percentages.

conductor and pipe wall temperatures comparing the improved model and full FEA calculation. The largest deviation between the improved model and the FEA with full convection calculation is 0.3 °C for the conductor and pipe wall temperatures. The same deviations are tabulated in Table II for different ratios of the conductor and pipe radii. The small deviation found for r_i/r_o = 0.5 is confirmed for both small (0.1) and large (0.9) ratios.

In practice the calculation time is at least 30 times longer for full FEA calculations compared to the simplified model, as full FEA requires a parametric sweep with increasing current to ensure convergence of the calculations. This is not a constraint for the simplified model, and a solution can be obtained directly from a single calculation.

B. Triangular and Cradle Formation

In many cases it is common practice to put the three cables of a three-phase circuit in the same pipe, arranged in a triangular or cradle formation. The simplified model has thus been compared to full FEA calculations including convection to test the validity for these relevant geometries. A current corresponding to 90 °C maximum conductor temperature in the simplified model was applied to both formations, 362 A for the triangular formation and 368 A for the cradle formation. An equivalent cable diameter multiplication factor of 2.15 according to IEC 60287-2-1 [2] was used, and the effective r_i/r_o ratio was 0.51. Cable and pipe properties are given in Table VI in Appendix A.

TABLE III
COMPARISON OF SIMPLIFIED MODEL AND FULL FEA CALCULATIONS FOR TRIANGULAR FORMATION

	Triangular – I = 362 A				
	Q_{cond} [W/m]	T_{cond} [°C]	T_{bottom} [°C]	T_{side} [°C]	T_{top} [°C]
Simplified model	67.3	90.1	54.1	45.8	42.8
Full FEA	65.8	85.9 (-4.7 %)	50.7 (-6.3 %)	44.7 (-2.4 %)	44.6 (4.2 %)

TABLE IV
COMPARISON OF SIMPLIFIED MODEL AND FULL FEA CALCULATIONS FOR CRADLE FORMATION

	Cradle – I = 368 A				
	Q_{cond} [W/m]	T_{cond} [°C]	T_{bottom} [°C]	T_{side} [°C]	T_{top} [°C]
Simplified model	71.0	89.9	57.4	46.9	44.0
Full FEA	70.9	90.5 (0.7 %)	56.3 (1.9 %)	48.3 (3.0 %)	44.8 (1,8 %)

TABLE V
TEMPERATURE DEVIATIONS BETWEEN MEASURED AND THE PROPOSED MODEL AT THE MAXIMUM CURRENT (535 A) FOR THE 110 MM AND 160 MM PIPES

	110 mm		160 mm	
ΔT_{cond}	1.4 °C	1.7 %	1.5 °C	1.9 %
ΔT_{sheath}	-1.2 °C	-1.8 %	1.6 °C	2.4 %
ΔT_{pipe_top}	3.5 °C	9.1%	-0.3 °C	-0.9%
ΔT_{pipe_side}	1.1 °C	3.2 %	4 °C	12 %
ΔT_{pipe_bottom}	-4.4 °C	-10.6 %	-13.4 °C*	-43 %*

* It is likely that the thermocouple was not in good contact with the pipe wall for this measurement point.

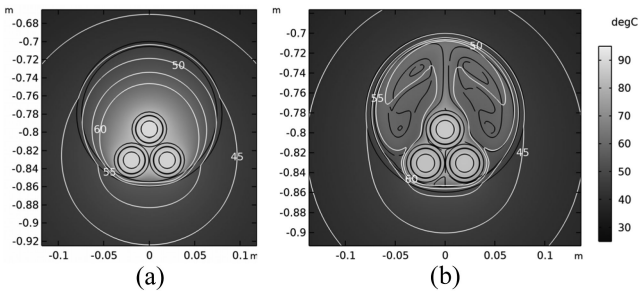

Fig. 11. (a) Temperature from simplified model and (b) temperature and airflow/streamlines from full FEA for triangular geometry.

The cradle formation has the most advantageous thermal properties, as all three cables are close to, and in contact with the pipe wall. In Table III and Table IV the calculated temperatures for the triangular and cradle formation are given, respectively, while images showing the temperature distributions and airflow are shown in Figs. 11 and 12. The largest deviation is found for the triangular formation with 4.7% lower conductor temperature

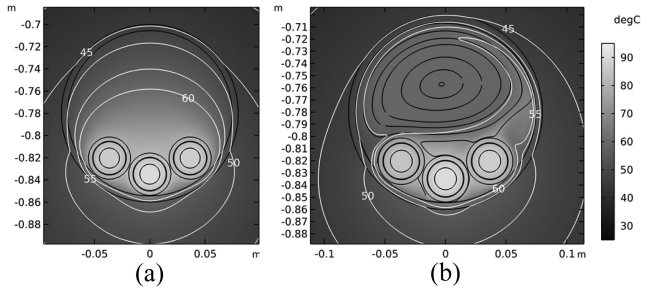

Fig. 12. (a) Temperature from simplified model and (b) temperature and airflow/streamlines from full FEA for cradle geometry.

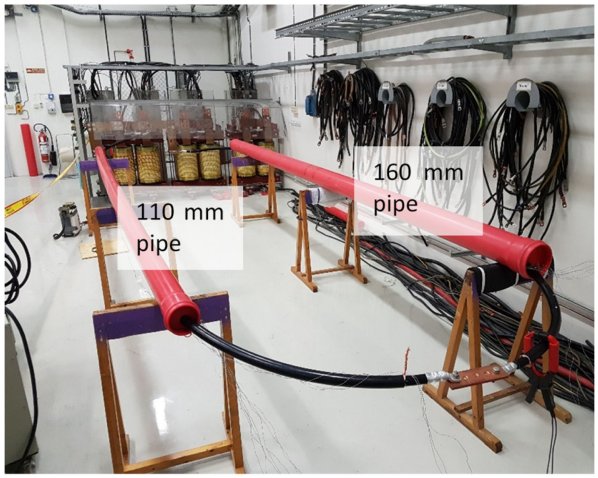

Fig. 13. Laboratory setup.

for the full FEA calculation, while the conductor temperature in the cradle formation is 0.7% higher for the full FEA calculation, demonstrating that the simplified model is applicable to geometries with three cables within the same pipe, although the resulting ampacity will be on conservative for the triangular formation.

It should be noted that solving the full FEA for the cradle formation in this case took two times longer than the triangular formulation. Although the cradle formation is geometrically symmetric about a vertical line, a non-symmetric flow field is established.

V. EXPERIMENTAL VERIFICATION IN THE LABORATORY

A. Background

A laboratory experiment was set up to verify the simplified model, as depicted in Fig. 13.

The cable was a TSLF 24 kV Al 240/35 and was laid in two 5 m long polypropylene pipe sections with outer the diameters of 110 mm and 160 mm, respectively. Both the cable type and the pipe diameters are representative for the configurations commonly used in the Norwegian distribution grid. The temperature was measured using thermocouples in the conductor, cable surface, and inside the pipe wall at the bottom, side and top, as shown in Fig. 14.

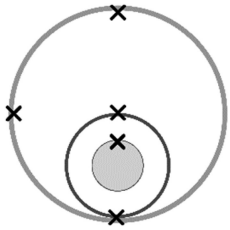

Fig. 14. Location of the thermocouples marked with crosses.

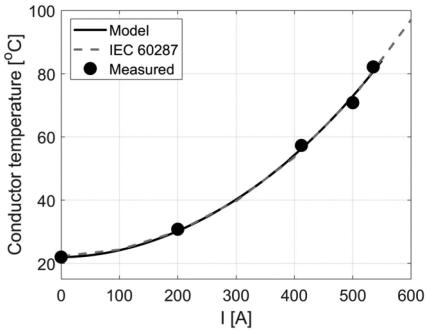

Fig. 15. Measured (black circles), IEC 60287 (broken grey) and model (black) conductor temperature for the cable in the 160 mm pipe.

Current at increasing levels were applied, and for each level, the temperatures were allowed to stabilize. The resistance of the conductor was also measured using a microohmmeter at the selected temperature levels to verify the conductor temperature measured with the thermocouples.

A model of the experimental setup was implemented in the FEA software applying the improved calculations presented in this paper. Further, the model included heat transfer to the surroundings by convection and radiation. Heat transfer from the outer pipe wall to the surrounding air was represented by a heat transfer coefficient with the values found in the literature for natural convection from a horizontal pipe [20], keeping in mind that this relation will not be accurate locally on the pipe wall. Radiation to the surroundings is diffuse and the emissivity of 0.8 was used.

B. Results

The measured conductor temperature as a function of the applied current (black dots), IEC 60287 formulation calculated in CYMCAP [21] (broken grey line) and corresponding calculated values for the proposed model (solid black line) are given for the 160 mm pipe in Fig. 15 and for the 110 mm pipe in Fig. 16. From the graphs it is seen that there is good correspondence between the measured and calculated conductor temperature values – both compared to the IEC formulation and the proposed model.

One of the features of the proposed model is to acquire a more accurate temperature distribution along the pipe wall. In Fig. 17 and Fig. 18, the temperatures for conductor, sheath, upper side and bottom positions on the pipe wall are plotted for 160 mm and 110 mm pipes, respectively.

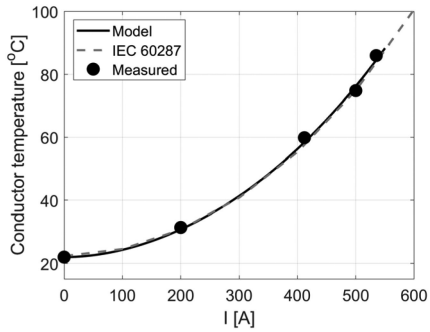

Fig. 16. Measured (black circles), IEC 60287 (broken grey) and model (black) conductor temperature for the cable in the 110 mm pipe.

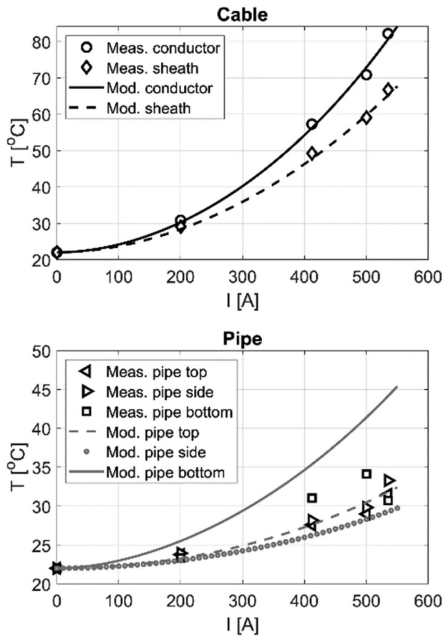

Fig. 17. Measured (symbols) and calculated (continuous and dotted lines) temperatures as functions of the applied current for cables conductor and sheath, and pipe wall upper, side and bottom positions for the 160 mm pipe.

In Table V the deviation between measured and calculated temperatures for the two cases are given. For the conductor the maximum deviation is 1.5 °C, whereas for the pipe temperatures the deviation is higher – maximum absolute deviation is 13.6 °C at the bottom surface of the 160 mm pipe. If the cable is not settled at the surface of the pipe – this could be the result. The other pipe measurements have absolute deviations below 4.4 °C.

VI. Experimental Verification in Field

A. Background

For further experimental verification of the model, a full-scale road-crossing has been constructed according to the specifications of the Norwegian Public Roads Administration regulations. A TSLF 24 kV Al 50/16 cable was installed in a 110 mm PE pipe and buried 109 cm below the ground surface in gravel. The surface was covered with asphalt, as shown in Fig. 19. The width

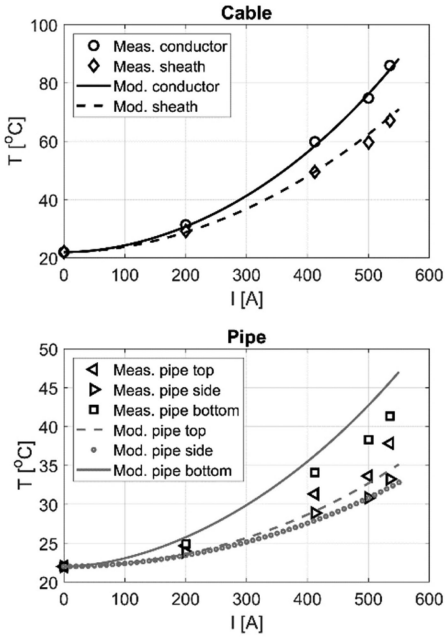

Fig. 18. Measured (symbols) and calculated (continuous and dotted lines) temperatures as functions of the applied current for cables conductor and sheath, and pipe wall upper, side and bottom positions for the 110 mm pipe.

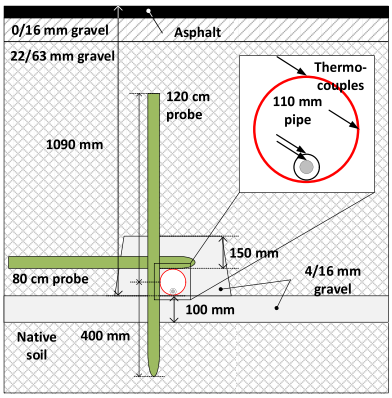

Fig. 19. Schematic of road crossing constructed according to Norwegian Road Authorities Specification Ref. [22].

at the trench base was 3.3 m and at the asphalt 6.5 m, giving a trapezoid shape of the trench. Details of the construction of the different layers in the road-crossing and ambient conditions have been reported in [22].

Thermal resistivity of the native clayey soil was measured in-situ with a Hukseflux transient needle probe at 0.6 m.K/W while the 4/16 mm gravel was measured with a steady-state laboratory setup (both setups described in [23]) at 3 m.K/W. The 22/63 gravel will have similar porosity as the 4/16 mm gravel; hence the same thermal resistivity was assumed. For the 0/16 mm and asphalt layers, the thermal resistivity was set to 1 m.K/W.

A step current starting at 260 A and rapidly decaying to 235 A was applied to the cable and the temperature in the conductor, cable surface and the side of the pipe was monitored as a function

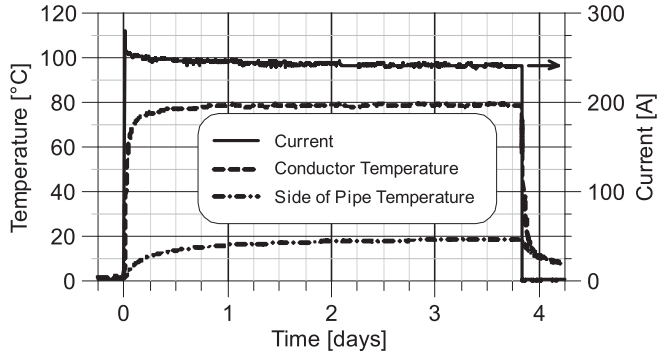

Fig. 20. Measured current and temperatures on conductor and side of the pipe.

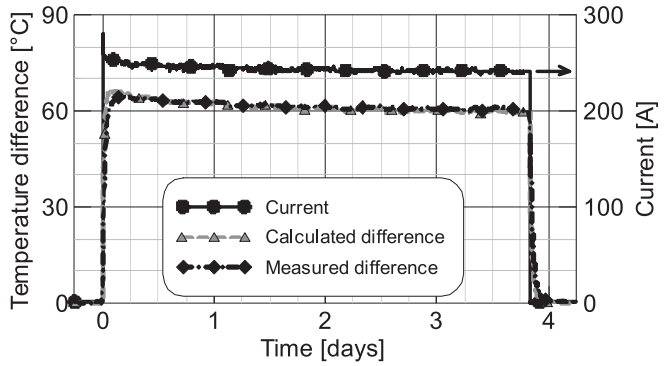

Fig. 21. Measured and calculated temperature difference between conductor and pipe wall and applied current.

of time with the thermocouples. Position of the thermocouples are shown in the insert of Fig. 19.

B. Results

The measured temperature in the conductor and on the pipe wall is shown in Fig. 20, together with the applied current. The calculated and measured difference in the temperature between the conductor and side of the pipe is shown in Fig. 21.

It should be noted that the measured temperatures were consistently lower compared to calculated values for the field experiment, likely due to water in the base layer of the trench or decreased thermal resistivity of the gravel in-situ compared to laboratory measurements. By taking the temperature difference between the pipe wall and the conductor, the minor deviation in thermal properties outside the pipe is to a large degree cancelled out. The deviation between measured and calculated temperature difference between the pipe wall and the conductor is below 2 °C and thus demonstrates that the proposed model is accurate for cables in buried pipes.

VII. Discussion

The primary goal for this work was to develop a thermal model that accurately reproduces the temperature profile around a cable in a pipe buried in the ground, with as few simplifications as possible and, at the same time, exploiting the capabilities of the FEA. Thus, the thermal model places the cable at the bottom of

the pipe, which results in the highest temperature at the contact point (as occurs in real life).

It should be recognized that absolute contribution to the heat transfer by convection is not changed much by placing the cable at the bottom of the pipe. The reduction in convective heat transfer that is found is caused by the change in temperature distribution on the cable and pipe surfaces, i.e., the effective temperature difference is smaller.

The main challenge in determining a new correlation for the convective heat transfer is that the temperature distribution in the case with convection is different from the case where convection is suppressed (i.e., not allowed to occur). The approach described in [19] for determining convective heat transfer correlations for non-standard geometries can be a good starting point and a guide.

VIII. Conclusion

The results from the measurements show that the simplified model can predict the conductor temperature with an accuracy better than 1 °C compared to the full FEA calculation for the tested cases with a single cable in pipe. Cable-to-pipe diameter ratios in the range 0.1 to 0.9 was tested as these are considered the practical range of power cable installation in pipes. When comparing the simplified model with the measured values, the conductor temperature deviation is within 1.5 °C. For cases with three cables within the pipe, comparison of conductor temperature yielded a deviation of 4.2 °C (-4.7%) in triangular formation, and for the cradle formation the deviation was 0.6 °C (0.7%).

The temperature distribution on the pipe wall is reproduced with a smaller accuracy, but still this model provides significant improvement for practical purposes compared to the IEC calculations and computational heavy full FEA models. The reason for the observed deviation is likely that the heat transfer coefficient varies tangentially along the pipe wall. The coefficient will be large where the air boundary layer is thin (under the cable) and smaller where the boundary layer is thicker (on the sides and the top of the cable). In the model, a global heat transfer coefficient was used.

The deviation in temperatures for single cable and cradle formation are negligible compared to the effect that variations in laying geometry and thermal properties of backfill materials can have. For triangular formation the deviation is higher than for the single cable and cradle formations, but the simplified model will in many cases improve accuracy compared to IEC methods and efficiency compared to full FEA calculations. More accurate calculations on complex geometries with multiple pipes can efficiently be achieved compared to the isothermal case due to the more realistic temperature distribution on the pipe wall.

Another advantage for the applicability of the simplified model is that ensuring convergence of the solution do not need to be considered. Even if the same input parameters must be entered, the simplified model makes ampacity calculations of cables in pipes available to a larger audience, especially if the general input parameters are given in a predefined application or interface.

Appendix A

TABLE VI
Cable and Pipe Dimensions for Lab Experiment

Cable properties	
Conductor cross section	240 mm^2
Conductor diameter	18.2 mm
Cable outer diameter	38.2 mm
Screen cross section	35 mm^2*
Pipe 1	
Outer diameter	110 mm
Wall thickness	5 mm
Pipe 2	
Outer diameter	160 mm
Wall thickness	5.5 mm

*Standardized value

TABLE VII
Cable and Pipe Dimensions for Full-Scale Experiment

Cable properties	
Conductor cross section	50 mm^2
Conductor diameter	18.2 mm
Cable outer diameter	38.2 mm
Screen cross section	16 mm^2*
Pipe 1	
Outer diameter	110 mm
Wall thickness	5 mm

*Standardized value

References

[1] G. J. Anders, *Rating of Electric Power Cables: Ampacity Computations For Transmission, Distribution, and Industrial Applications*, New York, NY, USA: Wiley, 1997.

[2] *IEC Electric Cables – Calculation of the Current Rating – Part 2: Thermal Resistance – Section 1: Calculation of the Thermal Resistance*, International Electrotechnical Commission Standard 60287-2-1, 2015.

[3] A. Sedaghat, H. Lu, A. Bokhari, and F. León, "Enhanced thermal model of power cables installed in ducts for ampacity calculations," *IEEE Trans. Power Del.*, vol. 33, no. 5, pp. 2404–2411, Oct. 2018.

[4] M. Z. Degefa, M. Lehtonen, and R. J. Millar, "Comparison of air-gap thermal models for MV power cables inside unfilled conduit," *IEEE Trans. Power Del.*, vol. 27, no. 3, pp. 1662–1669, Jul. 2012.

[5] G. D. Raithby and K. G. T. Hollands, "A general method of obtaining approximate solutions to laminar and turbulent free convection problems," in *Advances in Heat Transfer*, T. F. Irvine and J. P. Hartnett, Eds. Amsterdam, The Netherlands: Elsevier, 1975, pp. 265–315.

[6] X. Lu, A. X. Zhao, J. B. Deng, G. J. Zhang, P. Yu, and S. J. Yao, "Calculation of distribution cable steady and transient temperature field in ducts," in *Proc. China Int. Conf. Electricity Distrib.*, 2014, pp. 1280–1283.

[7] C. Fu, W. Si, L. Zhu, Y. Liang, and H. Li, "Rapid transfer matrix-based calculation of steady-state temperature rises in cable ducts containing groups of three phase cable," *IEEE Power Energy Technol. Syst. J.*, vol. 6, no. 3, pp. 208–213, Dec. 2019.

[8] C. Fu and Y. Liang, "Fast calculation of steady temperature rise for running Three-phase cable group in ducts based on transfer matrix," in *Proc. IEEE Elect. Power Energy Conf.*, 2019, pp. 1–6.

[9] F. D. Leon, "Major factors affecting cable ampacity," in *Proc. IEEE Power Eng. Soc. Gen. Meeting*, 2006, Art. no. 6.

[10] P. Vaucheret, R. A. Hartlein, and W. Z. Black, "Ampacity derating factors for cables buried in short segments of conduit," *IEEE Trans Power Del.*, vol. 20, no. 2, pp. 560–565, Apr. 2005.
[11] J. Neher and M. McGrath, "The calculation of the temperature rise and load capability of cable systems," *Trans. Amer. Inst. Elect. Engineers. Part III: Power App. Syst.*, vol. 76, no. 3, pp. 752–772, Oct. 1957.
[12] G. Liu *et al.*, "An improved analytical thermal rating method for cables installed in short-conduits," *Int. J. Electr. Power Energy Syst.*, vol. 123, Dec. 2020, Art. no. 106223.
[13] E. Eberg, K. Espeland, S. M. Hellesø, S. Hvidsten, and K. T. Solheim, "Development of a web-based user-friendly cable ampacity calculation tool," in *Proc. CIRED 2019 Conf.*, 2019, Art. no. 2117.
[14] W. M. Rohsenow, J. P. Hartnett, and E. N. Ganic, *Handbook of Heat Transfer Fundamentals*, 2nd ed. W. M. Rohsenow, J. P. Hartnett, and Y. I. Cho, Eds. New York, NY, USA: McGraw Hill, 1985.
[15] F. P. Incropera, D. P. Dewitt, T. L. Bermgan, and A. S. LAvine, *Fundamentals of Heat and Mass Transfer*, 6th ed. Hoboken, NJ, USA: Wiley, 2007.
[16] T. H. Kuehn and R. J. Goldstein, "An experimental study of natural convection heat transfer in concentric and eccentric horizontal cylindrical annuli," *J. Heat. Transfer.*, vol. 100, no. 4, pp. 635–640, Nov. 1978.
[17] P. Teertstray and M. M. Yovanovichz, "Comprehensive review of natural convection in horizontal circular annuli," in *Proc. 7th AIAA/ASME Joint Thermophys. Heat Transfer Conf.*, 1998, pp. 12–17.
[18] J. Francis, M. T. Itamura, S. Webb, and D. James, *CFD Calculation of Internal Natural Convection in the Annulus between Horizontal Concentric Cylinders*. New York, NY, USA: US Dept. Energy, 2002.
[19] J. Francis, M. T. Itamura, S. W. Webb, and D. L. James, *CFD Modeling of Natural Convection Heat Transfer and Fluid Flow in Yucca Mountain Project (YMP) Enclosures*. New York, NY, USA: US Dept. Energy, 2003.
[20] S. W. Churchill and H. H. S. Chu, "Correlating equations for laminar and turbulent free convection from a horizontal cylinder," *Int. J. Heat Mass Transf.*, vol. 18, no. 9, pp. 1049–1053, 1975.
[21] CYME International T&D, "Cymcap," 2021. [Online]. Available: https://www.cyme.com/software/cymcap/
[22] E. Eberg, K. Espeland, S. M. Hellesø, and S. Hvidsten, "Full-scale case study of a road crossing thermal bottleneck in a buried medium-voltage cable installation," in *Proc. CIRED - Open Access Proc. J.*, 2017, pp. 194–197.
[23] E. Eberg, K. Espeland, and K. Rieksts, "Estimation of the thermal resistivity of backfill materials using a practical approach," in *Proc. Jicable'19 - 10th Int. Conf. Power Insulated Cables: Proc., Versailles*, 2019, pp. 1–6.

Svein M. Hellesø received the M.Sc. degree from the Norwegian University of Science and Technology (NTNU), Trondheim, Norway, in 1999, and the Ph.D. degree in electrical engineering, with focus on vibrations on overhead lines, from NTNU, in 2005. During 2000–2001, he was a Researcher with SINTEF Energy Research, Norway. He then re-joined SINTEF Energy Research and works on R&D projects focusing on mechanical and thermal behaviour of and condition assessment of components in the electrical grid.

Espen Eberg received the M.Sc and Ph.D. degrees from the Norwegian University of Science and Technology, Trondheim, Norway, in 2007 and 2011, respectively. His work focused on nanofabrication and transmission electron microscopy studies of ferroelectric materials and structures. He currently holds a position as a Research Scientist with SINTEF Energy Research, where he conducts R&D projects focusing on condition assessment of electric power apparatus and ampacity calculations. He is also the Project Manager of Norwegian National Research Infrastructure ElpowerLab.